Natural occurrence and synthesis of two new postspinel polymorphs of chromite

Ming Chen*†, Jinfu Shu‡, Ho-kwang Mao‡, Xiande Xie*, and Russell J. Hemley‡

*Guangzhou Institute of Geochemistry, Chinese Academy of Sciences, Wushan, Guangzhou 510640, China; and ‡Geophysical Laboratory, Carnegie Institution of Washington, 5251 Broad Branch Road, NW, Washington, DC 20015

Contributed by Ho-kwang Mao, October 12, 2003

A high-pressure polymorph of chromite, the first natural sample with the calcium ferrite structure, has been discovered in the shock veins of the Suizhou meteorite. Synchrotron x-ray diffraction analyses reveal an orthorhombic $CaFe_2O_4$-type (CF) structure. The unit-cell parameters are $a = 8.954(7)$ Å, $b = 2.986(2)$ Å, $c = 9.891(7)$ Å, $V = 264.5(4)$ Å^3 ($Z = 4$) with space group *Pnma*. The new phase has a density of 5.62 g/cm^3, which is 9.4% denser than chromite-spinel. We performed laser-heated diamond anvil cell experiments to establish that chromite-spinel transforms to CF at 12.5 GPa and then to the recently discovered $CaTi_2O_4$-type (CT) structure above 20 GPa. With the ubiquitous presence of chromite, the CF and CT phases may be among the important index minerals for natural transition sequence and pressure and temperature conditions in mantle rocks, shock-metamorphosed terrestrial rocks, and meteorites.

Forty years ago, in search of denser polymorphs of the then newly discovered silicate spinel (ringwoodite) and modified spinel (wadsleyite) that are stable at the pressure and temperature (*P-T*) conditions of the Earth's transition zone, Ringwood (1, 2) proposed orthorhombic $CaFe_2O_4$-type (CF) and $CaTi_2O_4$-type (CT) structures as the top candidates for "postspinel" transitions in the Earth's mantle (Fig. 1). Although ferromagnesian silicate spinels were later found to break down to simple oxides (3) or stishovite plus perovskite (4), several postspinel oxides convert to a single phase with the CF or CT structure (1, 2, 5–12). Neither dense postspinel polymorphs nor silicate perovskites, however, have been discovered in nature and confirmed as new minerals. Many natural high-pressure minerals presumably predominating in the Earth's mantle have been found mainly in the shock-metamorphosed meteorites, which include ringwoodite, wadsleyite, silicate ilmenite, magnesiowüstite, (Na,K)$AlSi_3O_8$-hollandite, and poststishovite polymorphs (13–19). Special *P-T* conditions developed in the impacted meteorites, for instance, a long duration of high-pressure and -temperature up to several seconds and quenching under pressure, play an important role in the formation and preservation of high-pressure phases (16). It makes the naturally shock-metamorphosed meteorites a window for discovery of new high-pressure minerals and for investigation of the constituents in the deep Earth. Preliminary examination of the Suizhou meteorite has recently revealed a shock-metamorphosed CT polymorph of chromite composition (20). In this article, we report the identification of a previously uncharacterized CF polymorph of chromite in the same meteorite. High *P-T* experiments demonstrate that both CF and CT are indeed quenchable polymorphs of chromite formed above 12.5 and 20 GPa, respectively.

The Suizhou meteorite is a moderately shock-metamorphosed L6-chondrite, and a shock stage S5 was estimated for the meteorite according to the classification of shock metamorphism (21). The meteorite contains shock-produced melt veins ranging from 20 to 200 μm in width with a bulk chondritic composition. Major rock-forming minerals in the host meteorite are olivine, pyroxene, plagioclase, kamacite, taenite, and troilite. Accessory minerals include chromite, apatite, and whitlockite. Both olivine and pyroxene display moderate mosaic texture, and plagioclase was partially shock-melted and quenched to maskelynite, a plagioclase glass. The shock veins contain abundant high-pressure minerals (ringwoodite, majorite, magnesiowüstite, $NaAlSi_3O_8$-hollandite, and majorite-pyrope garnet solid solution) for which the shock-produced pressure and temperature of 20–22 GPa and ≈2,000°C is inferred (20, 22–24).

Methods

To investigate the *P-T* conditions for the formation of the high-pressure polymorphs of chromite, we performed a series of synthesis experiments at pressures from 7.5 to 25 GPa and at a temperature of 2,000°C, using laser-heated diamond anvil cells. A natural crystal of chromite with a similar chemical composition as the chromite in the Suizhou meteorite was used as the starting material, which contains 5.85 wt % MgO, 3.44 wt % Al_2O_3, 0.16 wt % TiO_2, 0.12 wt % V_2O_5, 59.69 wt % Cr_2O_3, 0.65 wt % MnO, 30.11 wt % FeO, and 100.02 wt % in total. Chromite samples were ground to a grain size of <1 μm. NaCl was used for the pressure medium in the sample chamber. A ruby grain of ≈3–5 μm in size was placed in the sample chamber for pressure determination (25). We compressed the sample to pressures 7.5, 10, 12.5, 15, 17.5, 20, and 25 GPa at room temperature. A double-sided laser heating system was used to heat the sample from both sides of the cell (26). The heating temperature of samples (2,000°C) was determined by measuring the thermal emission with a spectrometer/charge-coupled device detector system. After heating, the samples were decompressed and mounted on glass slides for x-ray analysis.

Polished thin sections of the Suizhou meteorite were prepared from the shock-vein-bearing fragments. The petrology and chemical compositions of the samples were investigated by optical microscopy, scanning electron microscopy in back-scattered electron mode, and electron microprobe. Both the meteorite samples and the quenched products recovered from high *P-T* experiments were analyzed by synchrotron x-ray diffraction for phase identification and crystal structure determination. X-ray diffraction measurements were conducted at the X17C superconducting wiggler beamline of the National Synchrotron Light Source, Brookhaven National Laboratory (Upton, NY). Energy-dispersive x-ray diffraction was used in the experiments. The primary x-ray beam, 8×20 μm, was directed through the sample on the glass slides, and diffraction data were collected with a solid-state Ge detector at a fixed 2θ angle of 15°. The quenched samples also were analyzed with monochromatic x-ray and a charge-coupled device detector that yielded the same results.

Results

Our experiments indicate that chromite-spinel transforms to the CF structure above 12.5 GPa and to the CT structure above 20

Abbreviations: CF, $CaFe_2O_4$-type; CT, $CaTi_2O_4$-type; *P-T*, pressure and temperature; ρ, density.

†To whom correspondence should be addressed. E-mail: mchen@gig.ac.cn.

© 2003 by The National Academy of Sciences of the USA

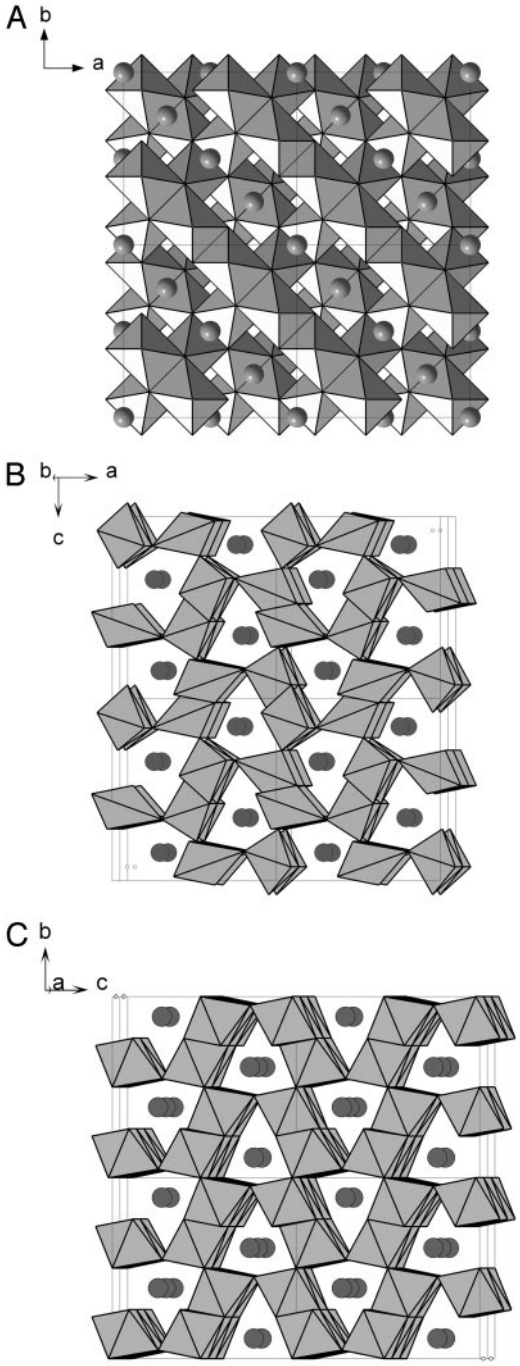

Fig. 1. Schematic view of spinel (*A*), CF (*B*), and CT (*C*) structures. The spinel structure has octahedral and tetrahedral sites. In the CF and CT structures, a compact three-dimensional network is formed by edge- and corner-sharing octahedra, with hollow channels parallel to the *b* axis (CF structure) and the *a* axis (CT structure), respectively, where the large Ca cations are located. These two structures contain dodecahedral and octahedral sites; the difference between the two structures lies in slight modifications of the polyhedral linkage. There are two types of FeO_6 octahedral sites in the CF structure and one type of FeO_6 octahedral site in the CT structure.

GPa. The *P-T* conditions for synthesizing the CT phase are coincident with the estimation based on the high-pressure mineral assemblage of shock veins of the Suizhou meteorite (20, 23, 24). Both high-pressure phases are quenchable on releasing *P-T* to ambient conditions. We synthesized a pure CT phase and a CF phase with some residue of chromite. A total of 20 x-ray

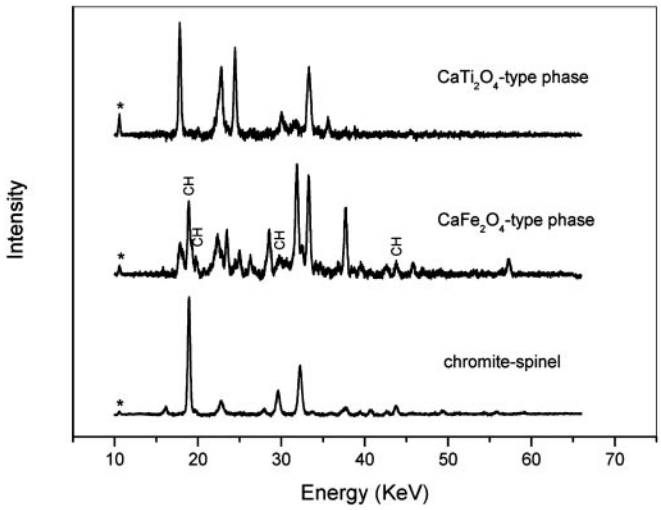

Fig. 2. X-ray diffraction patterns from chromite-spinel, CF, and CT phases. The peaks labeled with CH are from the residue of starting material chromite-spinel. *, Escape peaks.

reflections from the CF phase and 21 reflections from the CT phase were collected in addition to those from chromite (Fig. 2). The x-ray diffraction pattern of the quenched CF polymorph was indexed to give lattice parameters $a = 8.955(7)$ Å, $b = 2.985(2)$ Å, $c = 9.909(7)$ Å, $V = 264.9(4)$ Å^3 ($Z = 4$), density (ρ) = 5.61 g/cm^3, and space group *Pnma* (Table 1), and that of the CT polymorph, $a = 9.467(5)$ Å, $b = 9.550(7)$ Å, $c = 2.905(2)$ Å, $V = 262.6(4)$ Å^3 ($Z = 4$), $\rho = 5.65$g/cm^3, and space group *Cmcm* (Table 2). In comparison, lattice parameters of the starting chromite are $a = 8.338(9)$ Å, $V = 579.7(3)$ Å^3 ($Z = 8$), and $\rho = 5.13$ g/cm^3. The densities of synthetic CF and CT polymorphs are

Table 1. Indexed peaks of the x-ray diffraction patterns and Miller indices collected from natural and synthetic CF polymorphs of chromite

	Natural		Synthetic	
h k l	d_{obs}, Å	d_{cal}, Å	d_{obs}, Å	d_{cal}, Å
2 3 0	2.656 (2)$_s$	2.6549	2.657 (2)$_s$	2.6581
2 4 0	2.166 (2)$_s$	2.1647	2.169 (1)$_w$	2.1676
3 0 1	2.108 (3)$_w$	2.1111	2.108 (3)$_w$	2.1110
4 2 0	2.039 (1)$_s$	2.0394	2.035 (5)$_s$	2.0402
2 5 0	1.807 (2)$_w$	1.8095	1.808 (4)$_s$	1.8122
4 4 0	1.660 (3)$_s$	1.6596	1.663 (2)$_s$	1.6610
2 6 0			1.550 (7)$_w$	1.5498
5 0 1	1.536 (5)$_s$	1.5359		
0 0 2	1.498 (6)$_w$	1.4931	1.494 (2)$_s$	1.4928
5 2 1	1.468 (2)$_w$	1.4668	1.467 (1)$_w$	1.4670
1 6 1	1.425 (2)$_s$	1.4249	1.429 (2)$_s$	1.4267
2 6 1	1.372 (1)$_w$	1.3737	1.370 (5)$_w$	1.3753
3 0 2	1.336 (1)$_w$	1.3354	1.334 (1)$_w$	1.3352
3 2 2	1.285 (4)$_w$	1.2892	1.287 (2)$_w$	1.2892
1 4 2	1.267 (2)$_s$	1.2654	1.263 (2)$_s$	1.2658
4 2 2	1.206 (2)$_w$	1.2047	1.206 (2)$_w$	1.2048
5 2 2	1.117 (1)$_w$	1.1172	1.115 (2)$_w$	1.1172
5 3 2	1.081 (2)$_w$	1.0832	1.084 (1)$_w$	1.0833
4 2 3	0.893 (1)$_w$	0.8945	0.891 (3)$_w$	0.8945
1 6 3	0.848 (1)$_w$	0.8483	0.849 (1)$_w$	0.8486
6 0 3	0.828 (2)$_w$	0.8281	0.829 (1)$_w$	0.8280

d_{obs} and d_{cal} are observed and calculated *d* values, respectively. $_s$, strong diffraction peak; $_w$, weak diffraction peak.

Table 2. Indexed peaks of the x-ray diffraction patterns and Miller indices collected from synthetic and natural CT polymorphs of chromite

	This experiment		Suizhou meteorite*	
h k l	d_{obs}, Å	d_{cal}, Å	d_{obs}, Å	d_{cal}, Å
1 1 1	2.665 $(2)_s$	2.6667	2.674 $(1)_s$	2.6754
0 4 0	2.383 $(4)_w$	2.3876	2.389 $(2)_w$	2.3905
2 4 0	2.130 $(1)_w$	2.1318	2.130 $(3)_w$	2.1336
4 2 0	2.120 $(1)_w$	2.1206	2.122 $(2)_w$	2.1203
3 1 1	2.086 $(1)_s$	2.0857	2.088 $(1)_s$	2.0895
3 2 1	1.946 $(5)_s$	1.9508	1.952 $(2)_s$	1.9542
1 4 1	1.807 $(3)_w$	1.8105	1.813 $(1)_w$	1.8144
4 4 0	1.678 $(2)_w$	1.6809		
5 0 1	1.584 $(2)_w$	1.5863	1.588 $(1)_w$	1.5875
5 1 1			1.566 $(1)_w$	1.5661
5 2 1	1.502 $(3)_w$	1.5054	1.506 $(1)_w$	1.5066
0 0 2	1.451 $(1)_w$	1.4525		
0 1 2	1.434 $(2)_w$	1.4360	1.439 $(2)_w$	1.4414
3 5 1	1.426 $(2)_s$	1.4242	1.424 $(2)_s$	1.4263
1 6 1	1.380 $(1)_w$	1.3810		
2 2 2	1.335 $(2)_w$	1.3334	1.337 $(1)_s$	1.3377
4 1 2	1.225 $(3)_w$	1.2277	1.229 $(2)_w$	1.2309
6 0 2			1.071 $(1)_w$	1.0706
8 0 0	1.184 $(1)_w$	1.1834		
2 6 2	1.045 $(1)_w$	1.0464	1.050 $(1)_w$	1.0490
6 3 2	1.010 $(3)_w$	1.0131	1.014 $(1)_w$	1.0149
6 4 2	0.978 $(3)_w$	0.9754	0.977 $(1)_w$	0.9771
1 2 3			0.947 $(1)_w$	0.9477
3 2 3			0.913 $(2)_w$	0.9119
3 3 3	0.889 $(1)_w$	0.8889	0.890 $(2)_w$	0.8918

d_{obs} and d_{cal} are observed and calculated *d* values, respectively. $_s$, strong diffraction peak; $_w$, weak diffraction peak.
*Data from ref. 20.

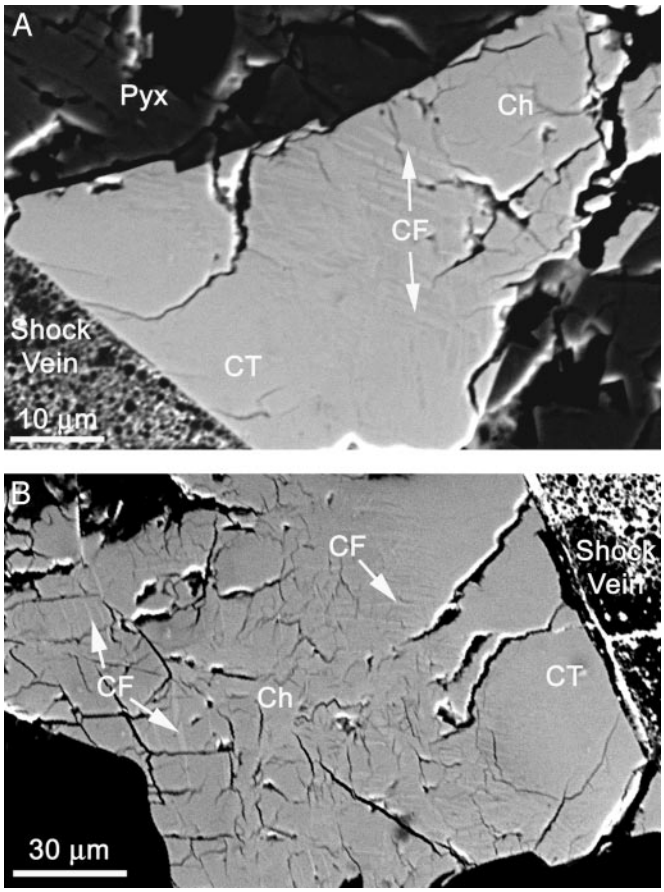

Fig. 3. Back-scattered electron (BSE) images of shock-metamorphosed chromite-spinel grains. (*A*) A chromite grain was transformed to a CT phase zone (CT) contacting with shock vein, and partially to a CF phase zone (CF) between the CT phase zone and the chromite zone (Ch) apart from the shock vein. The CF phase occurs as lamella-like slices associating with a chromite matrix, and two to three sets of slices are observed. On the image, both the CT and CF phases are brighter than chromite. Pyx, pyroxene. (*B*) BSE image showing that a high density of CF phase slices occurs in neighboring areas to the CT phase zone, but some slices distribute in the chromite zone apart from the shock vein.

9.4% and 10.1% denser than that of the original chromite, respectively.

Petrographic studies in the Suizhou meteorite demonstrate the existence of a gradient of shock-produced pressure and temperature from the shock veins to the neighboring host meteorite during the shock event. Some chromite grains in close association with the shock veins covered a shock-induced pressure gradient. Very recently, the CT polymorph of chromite was reported from these chromite grains, in addition to those occurring inside the shock veins (20). The electron backscattering images of these grains show three zones of distinct densities corresponding to the pressure gradient, i.e., CT phase zone close to the shock vein, chromite zone relatively apart from the vein, and a lamella-rich zone between CT phase zone and chromite zone (Fig. 3). It shows that the formation of the CT phase and lamella-like slices was highly pressure-dependent. Two to three sets of regular lamella-like slices in these grains clearly indicate that the produce of these slices may intimately associate with special crystallographic orientations and shock-produced deformation features of parent chromite-spinel phase.

Electron microprobe analyses of these three zones show a uniform chemical composition of chromite: 2.62 wt % MgO, 29.70 wt % FeO, 0.81 wt % MnO, 2.59 wt % TiO_2, 57.30 wt % Cr_2O_3, 5.97 wt % Al_2O_3, 0.97 wt % V_2O_3, and 99.93 wt % in total. The chemical formula of the mineral chromite is $(Fe_{0.84}Mg_{0.14}Mn_{0.02})(Cr_{1.58}Al_{0.26}V_{0.03}Fe_{0.03}Ti^{4+}_{0.07})_{1.97}O_4$. Our high *P-T* experiment indicates that the quenched CF and CT phases are difficult to distinguish with commonly used petrographic probes, such as petrographic microscopy, scanning electron microscopy, electron microprobe, and micro-Raman spectroscopy, but are clearly distinguishable by their characteristic x-ray diffraction patterns. We used a synchrotron x-ray beam to probe the shock chromite grain *in situ* in the thin-section mount of the Suizhou meteorite. We confirmed that a zone ranging from 20 to 30 μm in width in contact with the shock vein had transformed to a fine-grained polycrystalline aggregate with the CT structure identical to the CT phase synthesized experimentally (Table 2). We also confirmed that the clear zone at the low-pressure end has the usual chromite-spinel structure.

The lamella-like zone between the CT and spinel zones was previously interpreted as a mixture of CT and spinel phases (20). We focused the x-ray microprobe on this region and obtained the diffraction patterns distinct from the CT phase, which is consistent with a mixture of CF phase and spinel and trace amount of CT phase, with the fraction of spinel diminishing toward the shocked vein and the CT phase increasing toward the shocked vein (Fig. 4). The x-ray patterns collected from different orientations of sample show a polycrystalline nature of the lamellae-like slices, with a preferential crystallographic orientation in the microcrystalline CF phase. We collected a total of 20 x-ray reflections from the CF phase in addition to those from chromite (Table 1). They were indexed to an orthorhombic cell (7) with parameters $a = 8.954(7)$ Å, $b = 2.986(2)$ Å, $c = 9.891(7)$ Å, $V = 264.5(4)$ Å^3, and ($Z = 4$). The structure is identical to the

GEOLOGY

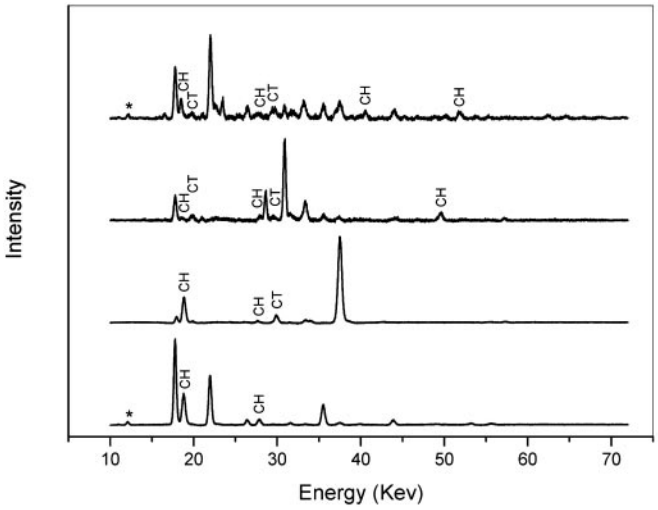

Fig. 4. X-ray diffraction patterns from natural CF phase. Each pattern was obtained at a different orientation of the sample. The peaks labeled with CH are from chromite-spinel and CT from CT phase. Other peaks that are unlabeled are from CF phase. *, Escape peaks.

synthetic CF phase in our high-pressure experiment. The calculated density of the natural CF phase is $\rho = 5.62$ g/cm^3, which is 9.4% denser than that of the chromite-spinel and is similar to the natural sample with the CT phase ($V = 263.8$ Å^3, $\rho = 5.63$ g/cm^3) (20). This is a natural $FeCr_2O_4$ polymorph with the CF structure.

Discussion

The occurrence of high-pressure polymorphs of chromite in the Suizhou meteorite supports a solid-state mechanism for the transformation of chromite to CF- and CT-structured phases. There is no evidence for an intermediate decomposition process, such as the postspinel transitions of $MgAl_2O_4$ (5, 7, 12). The results indicate that the solid-state phase transformation is, in general, a dominating mechanism for the formation of high-pressure minerals in naturally shocked meteorites (16). Chromite is a common accessory mineral occurring in most meteorites and in many mantle rocks. Dense polymorphs of microscopic accessory minerals offer rich information of the *P-T* history, but they are often overlooked unless the appropriate analytical probes and experimental simulations are applied. The experimentally calibrated CF and CT polymorphs of chromite could therefore be an ideal pressure gauge not only for shock-metamorphosed terrestrial rocks and meteorites but also for mantle rocks covering the important pressure range throughout the transition zone.

Our high *P-T* experiments indicate that nominal $FeCr_2O_4$ can adopt the CF and CT structures from the lower part of upper mantle (≈380 km) to the upper part of lower mantle (≈680 km). The natural CF- and CT-structured $FeCr_2O_4$ phases in the Suizhou meteorite contain Al_2O_3 (6.0 wt %) and MgO (2.6 wt %), in which the Al^{3+} and Cr^{3+} cations occupy octahedral sites, whereas the Mg^{2+} and Fe^{2+} are located in the dodecahedral sites. Previous experiments showed that $MgAl_2O_4$ might also take the CF or CT structures at specific *P-T* conditions (5, 7, 9, 12). This finding has implications for the widespread cation substitution of Al for Cr and between Mg and Fe in this structure type. Considering the ubiquitous presence of spinel minerals, their extensive range of composition, and their composition dependence of the transition pressure, the spinel-CF-CT transition series could potentially provide a comprehensive pressure-gauge system over an extended range. Furthermore, in addition to the Cr, Al, Mg, and Fe substitution in natural chromite, the CF and CT phases are likely to incorporate Ca, Ti, Fe, Na, Si (as in $CaFe_2O_4$, $CaTi_2O_4$, and $NaAlSiO_4$), and possibly other divalent and trivalent transition elements and rare earth elements, and thus have major effects on element partitioning of the deep Earth geochemistry.

We thank M. Akaogi, N. Funamori, S. Gramsch, and S. Shim for valuable comments; J. Hu for help with x-ray diffraction; X17C at National Synchrotron Light Source and High-Pressure Collaborative Access Team at Advanced Photon Source, Argonne National Laboratory, for synchrotron beam time; and Chinese Academy of Sciences (Hundred Talents Program, KZCX3-SW-123), National Science Foundation of China, U.S. National Science Foundation, and U.S. Department of Energy for support.

1. Reid, A. F. & Ringwood, A. E. (1969) *Earth Planet. Sci. Lett.* **6,** 205–208.
2. Reid, A. F. & Ringwood, A. E. (1970) *J. Solid State Chem.* **1,** 557–565.
3. Bassett, W. A. & Ming, L. C. (1972) *Phys. Earth Planet. Inter.* **6,** 154–160.
4. Shim, S., Duffy, T. S. & Shen, G. (2001) *Nature* **411,** 571–574.
5. Funamori, N., Jeanloz, R., Nguyen, J. H., Kavner, A., Caldwell, W. A., Fujino, K, Miyajima, N., Shinmei, T. & Tomioka, N. (1998) *J. Geophys. Res.* **103,** 20813–20818.
6. Liu, L. (1977) *Geophys. Res. Lett.* **4,** 183–186.
7. Irifune, T., Fujino, K. & Ohtani, E. (1991) *Nature* **349,** 409–411.
8. Yagi, Y., Suzki, T. & Akaogi, M. (1994) *Phys. Chem. Minerals* **21,** 12–17.
9. Akaogi, M., Hamada, Y., Suzuki, T., Kobayashi, M. & Okada, M. (1999) *Phys. Earth Planet. Inter.* **115,** 67–77.
10. Andrault, D. & Bolfan-Casanova, N. (2001) *Phys. Chem. Minerals* **28,** 211–217.
11. Wang, Z., O'Neill, H. S. C., Lazor, P. & Saxena, S. K. (2002) *J. Phys. Chem. Solids* **63,** 2057–2061.
12. Irifune, T., Naka, H., Sanehira, T., Inoue, T. & Funakoshi, K. (2002) *Phys. Chem. Minerals* **29,** 645–654.
13. Binns, R. A., Davis, R. J. & Reed, S. J. B. (1969) *Nature* **221,** 943–944.
14. Price, G. D., Putnis, A., Agrell, S. O. & Smith, D. G. W. (1983) *Can. Mineral.* **21,** 29–35.
15. Tomioka, N. & Fujino, K. (1999) *Am. Mineral.* **84,** 267–271.
16. Chen, M., Sharp, T. G., El Goresy, A., Wopenka, B. & Xie, X. (1996) *Science* **271,** 1570–1573.
17. Gillet, P., Chen, M., Dubrovinsky, L. & El Goresy, A. (2000) *Science* **287,** 1633–1636.
18. Sharp, T. G., El Goresy, A., Wopenka, B. & Chen, M. (1999) *Science* **284,** 1511–1513.
19. El Goresy, A., Dubrovinsky, L., Sharp, T. G., Saxena, S. K. & Chen, M. (2000) *Science* **288,** 1632–1634.
20. Chen, M., Shu, J., Xie, X. & Mao H. K. (2003) *Geochim. Cosmochim. Acta* **67,** 3937–3942.
21. Stöffler, D., Keil, K. & Scott, E. R. D. (1991) *Geochim. Cosmochim. Acta* **55,** 3845–3867.
22. Agee, C. B., Li, J., Shannon, M. C. & Circone, S. (1995) *J. Geophys. Res.* **100,** 17725–17740.
23. Xie, X., Chen, M. & Wang, D. (2001) *Eur. J. Mineral.* **13,** 1177–1190.
24. Xie, X., Minitti, M., Chen, M., Mao, H. K., Wang, D., Shu, J. & Fei, Y. (2002) *Geochim. Cosmochim. Acta* **66,** 2439–2444.
25. Mao, H. K., Bell, P. M., Shaner, J. W. & Steinberg, D. J. (1978) *J. Appl. Phys.* **49,** 3276–3283.
26. Ma, Y., Mao, H. K., Hemley, R. J. & Gramsch, S. A. (2001) *Rev. Sci. Instrum.* **72,** 1302–1305.